SUPPORTING INFORMATION

Title: Unraveling molecular recognition of glycan ligands by Siglec-9 via NMR spectroscopy and molecular dynamics modeling

Author list: Unai Atxabal[1], Corwin Nycholat[2], Johannes Pröpster[3], Andrea Fernández[1], Iker Oyenarte[1], Maria Pia Lenza[1],; Antonio Franconetti[1], Cátia O. Soares[4,5], Helena Coelho[4,5], Filipa Marcelo[4,5], Mario Schubert[3,6], James C. Paulson[2], Jesús Jiménez-Barbero*,[1,7,8,9] and June Ereño-Orbea*[1,7]

Author address:

[1]Chemical Glycobiology lab, Center for Cooperative Research in Biosciences (CIC bioGUNE), Basque Research and Technology Alliance (BRTA), 48160 Derio, Bizkaia, Spain.

[2]Departments of Molecular Medicine and Immunology & Microbiology, The Scripps Research Institute, 10550 North Torrey Pines Road, La Jolla, California 92037, United States.

[3] Institute of Molecular Biology and Biophysics, ETH Zurich, 8093 Zurich, Switzerland

[4]Associate Laboratory i4HB - Institute for Health and Bioeconomy, NOVA School of Science and Technology, Universidade NOVA de Lisboa, 2829-516 Caparica, Portugal.

[5]UCIBIO, Department of Chemistry, Faculdade de Ciências e Tecnologia, Universidade NOVA de Lisboa, 2829-516 Caparica, Portugal.

[6]Dept. of Biosciences and Molecular Biology, University of Salzburg, Hellbrunnerstrasse 34, 5020 Salzburg, Austria.

[7]Ikerbasque, Basque Foundation for Science, Euskadi Pl., 5, 48009 Bilbao, Biscay, Spain

[8]Department of Organic & Inorganic Chemistry, Faculty of Science and Technology, University of the Basque Country, EHU-UPV, 48940 Leioa, Bizkaia, Spain.

[9]Centro de Investigacion Biomedica En Red de Enfermedades Respiratorias, Av. Monforte de Lemos, 3-5. Pabellón 11. Planta 0. 28029 Madrid, Spain.

* Correspondence: Jesús Jiménez-Barbero (jjbarbero@cicbiogune.es), June Ereño-Orbea (jereno@cicbiogune.es)

Table of contents:

SUPPORTING MATERIALS AND METHODS

Ligands

The synthesis of glycomimetics ^{BTC}Neu5Ac and ^{MTTS}Neu5Ac has already been described[1,2]. The natural glycan ligand α2,3SLN was synthesized as described here[2]. The synthesis of the natural ligand 6-*O*-sulfo sLeX is described in this publication[3]. α2,6SLN (GLY084-2-90%)and sLeX (GLY047-80%) were purchased from Elicityl.

Cloning, expression and purification of Siglec-9

The pET-43.1(a) plasmid coding Siglec-9 (UniprotKB Q9NYZ4) V-Ig set domain (amino acid residues 18−144) (Siglec-9_{d1})[4] contains C36S mutation and 6×His tag. The DNA was synthesized and purchased from GenScript. The expression in Rosetta-gami B (DE3) *E.coli* competent cells (Novagen) was conducted as described elsewhere[5]. Siglec-9_{d1} was purified from the inclusion bodies from the lysed cells after solubilization with 6M guanidium chloride and refolding by subsequently decreasing the denaturing conditions. Purification was conducted using nickel affinity column, followed by size exclusion chromatography (Superdex 75; GE Healthcare). The purity of the protein was analyzed by SDS-PAGE and mass spectrometry, and the protein folding was determined by a ^{1}H-^{15}N-HSQC NMR experiment.

The full-length extracellular domain (ECD) of Siglec-9_{d1d3} (UniprotKB Q9Y366, residues 18–344) with a removable C-terminal VENUS protein[6] was codon-optimized for expression in human cells and synthesized by GenScript®. The construct was subcloned into the pHLsec vector[7] using restriction enzymes AgeI and KpnI, such that a 6x His-tag was at the C terminus of the construct to facilitate affinity purification. Siglec-9_{d1-d3}-mVenus was transiently transfected into HEK293F (Thermo Fisher Scientific) suspension cells. Cells were split in 200 ml cultures at 0.8×10^6 cells per ml. 50 µg of DNA was added to the cells in a 1:1 ratio with transfection reagent FectoPRO (Polyplus Transfections). Cells were incubated at 37 °C, 130 rpm, 8% CO_2 and 70 % humidity for 6–7 days. After this period, cells were harvested by centrifugation at 5000× g for 20 min, and supernatants were retained and filtered using a 0.45 µm Steritop filter (EMD Millipore). Supernatants were passed through a HisTrap Ni-NTA column (GE Healthcare) and eluted in 20 mM Tris pH 8.0, 300 mM NaCl buffer with an increasing gradient of imidazole (up to 500 mM). The fractions containing Siglec-9_{d1-d3}-mVenus were pooled and separated on a Superdex 200 Increase size exclusion column (GE Healthcare) in saline-phosphate buffer (sodium phosphate 20 mM, NaCl 150 mM, pH 7.4). Before NMR studies Siglec-9_{d1d3}-mVenus samples were freeze-dried to get rid of the H_2O.

NMR backbone assignment

NMR spectra were recorded on Bruker AVIII 500-, 600-, 700-, 750-, and 900-MHz spectrometers (all equipped with a cryogenic probe, except for AVIII 750 MHz) at 293 K. Samples were measured in 20 mM potassium phosphate, 40 mM NaCl at pH 7.0 with a protein concentrations of 0.27 mM in a 5 mm Shigemi-NMR tube, containing 10% (vol/vol) D_2O. Sequence-specific assignment of protein backbone resonances was achieved through 2D ^{1}H,^{15}N-HSQC, 3D HNCA, 3D HNCACB, 3D CBCA(CO)NH, 3D HNCO, 3D HN(CO)CA with the support of a 3D ^{15}N-edited NOESY-HSQC spectrum. The NOESY experiment was recorded using a mixing time of 120 ms. Spectra were processed in TopSpin 3.0 (Bruker) and analyzed in Sparky (T. D. Goddard and D. G. Kneller, SPARKY 3, University of California, San Francisco). The ^{1}H chemical shifts are referenced to 2,2-dimethyl-2-silapentane-5-sulfonic acid (DSS) in an external sample of 2 mM sucrose and 0.5 mM DSS (Bruker). The ^{13}C and ^{15}N chemical shifts are indirectly referenced using scaling factors of 0.251449530 and 0.101329118, respectively.

Isothermal titration calorimetry

Titrations of Siglec-9_{d1} with ^{BTC}Neu5Ac and ^{MTTS}Neu5Ac were carried out in PBS solutions (sodium phosphate 20 mM, sodium chloride 150 mM, pH 7.4) by the addition of small aliquots (3-5 μL) of a solution of the sugar into a solution of the protein in the same buffer. The concentration of the sugar solutions was approximately 30 to 40 times more concentrated than receptor solutions (50 μM). The association constants and the thermodynamic parameters were obtained from the fit of the titration data to a single-site binding model using the MicroCal Origin 7 software.

SUPPORTING TABLES

Table S1. Epitope residues of α2,3SLN calculated from the ^{1}H STD-NMR experiment in the presence of Siglec-9$_{d1\text{-}d3}$ (1:40 molar ratio). The absolute STD (STD-AF) values were evaluated for the NMR signals of the ligand, using the proton signal with the strongest STD effect as reference. Consequently, the relative STD intensities (STD%) were then calculated, allowing us to map the ligand-binding epitope.[8,9]

Protons	STD-AF	STD-AF (%)
NHAc Neu5Ac	2.5	100
H4 Neu5Ac	1.8	74
H7 Neu5Ac	1.5	60
H6 Neu5Ac	1.4	55
H9R Neu5Ac	1.1	46
H8 Neu5Ac	1	40
H9R Neu5Ac	0.9	35
H5 Neu5Ac	0.9	35
H3eq Neu5Ac	0.8	32
H3ax Neu5Ac	0.7	27
H5Gal	0.6	26
H4Gal	0.6	26
H3Gal	0.5	21
H6Gal	0.4	16
H3Gal	0.5	19
H6 GlcNAc	0.2	6
H2GlcNAc	0.1	5

Table S2. Epitope residues of α2,6SLN calculated from the ^{1}H STD-NMR experiment in the presence of Siglec-9$_{d1-d3}$ (1:40 molar ratio). The absolute STD (STD-AF) values were evaluated for the NMR signals of the ligand, using the proton signal with the strongest STD effect as reference. Consequently, the relative STD intensities (STD%) were then calculated, allowing us to map the ligand-binding epitope.[8,9]

Protons	STD-AF	STD-AF (%)
NHAc Neu5Ac	1.5	100
H7Neu5Ac	0.7	49
H4Neu5Ac	0.7	46
H9proRNeu5Ac	0.6	39
H6Neu5Ac	0.4	29
H5Neu5Ac	0.4	29
H9proSNeu5Ac	0.4	25
H3axNeu5Ac	0.3	23
H8Neu5Ac	0.3	21
H3aqNeu5Ac	0.3	20
H4Gal	0.1	10
NHAc Gal	0.1	10
H6Gal	0.1	9

Table S3. Epitope residues of sLeX calculated from the ^{1}H STD-NMR experiment in the presence of Siglec-9_{d1-d3} (1:40 molar ratio). The absolute STD (STD-AF) values were evaluated for the NMR signals of the ligand, using the proton signal with the strongest STD effect as reference. Consequently, the relative STD intensities (STD%) were then calculated, allowing us to map the ligand-binding epitope. [8,9]

Protons	STD-AF	STD-AF (%)
NHAc Neu5Ac	2.4	100
H6 Neu5Ac	2.1	86
H9proR Neu5Ac	1.8	75
H5 Neu5Ac	1.3	54
H4 Neu5Ac	1.4	58
H4 Neu5Ac	1.4	56
H7 Neu5Ac	1.6	65
H9S Neu5Ac	1.2	49
H3ax Neu5Ac	0.7	29
H8 Neu5Ac	1.0	41
H3eq Neu5Ac	0.6	24
H4 Gal	0.6	25
H6 Gal	0.6	26
H3 Fuc	0.6	23
H6 Fuc	0.4	17
H3Gal	0.4	16
H6GlcNAc	0.3	12

Table S4. Epitope residues of ^{BTC}Neu5Ac calculated from the ^{1}H STD-NMR experiment in the presence of Siglec-9$_{d1-d3}$ (1:40 molar ratio). The STDmax and ksat were calculated by plotting the obtained STD-AF *vs* the applied saturation time and fitting the data to a monoexponential function, as shown in the Materials and Methods sections. STD-AF$_0$ was obtained by multiplying STDmax and ksat.

Protons	STDmax	ksat (s^{-1})	STD-AF$_0$	STD-AF$_0$ (%)
Horto/para Fenil	6.8	0.6	4.0	100
Hmeta Fenil/ Hmethyl Fenil	6.2	0.5	3.3	82
Htriazol	5.6	0.5	3.0	73
Hmethylene C5Neu5Ac	2.6	0.5	1.3	33
H8 Neu5Ac	3.5	0.4	1.6	39
H6 Neu5Ac	2.4	0.7	1.7	42
H7 Neu5Ac	2.4	0.3	0.6	15
H4 Gal	2.3	0.3	0.7	18
H9proR Neu5Ac	2.7	0.6	1.7	43
H5 Gal	1.3	0.5	0.6	16
H6 Gal	1.2	0.4	0.4	11
H6 Glc	1.3	0.2	0.3	8

Table S5. Epitope residues of ^{MTSS}Neu5Ac calculated from the ^{1}H STD-NMR experiment in the presence of Siglec-9$_{d1-d3}$ (1:40 molar ratio). The STDmax and ksat were calculated by plotting the obtained STD-AF *vs* the applied saturation time and fitting the data to a monoexponential function, as shown in the Materials and Methods sections. STD-AF$_0$ was obtained by multiplying STDmax and ksat.

Protons	STDmax	ksat (s^{-1})	STD-AF$_0$	STD-AF$_0$ (%)
H thiazol	4.6	0.3	1.2	100
H3 thiol	3.2	0.4	1.1	95
H4 thiol	3.2	0.4	1.1	95
CH3 thiazol	3.0	0.3	1.0	84
NHAc Neu5Ac	2.9	0.4	1.1	90
H3ax Neu5Ac	2.5	0.1	0.3	28
H3eq Neu5Ac	1.3	0.2	0.3	27
H7 Neu5Ac	1.5	0.5	0.7	60
H4 Gal	2.0	0.3	0.5	42
H9proR Neu5Ac	1.1	0.5	0.6	51
H8 Neu5Ac	1.5	0.3	0.5	44
H5 Neu5Ac	1.2	0.4	0.4	38
H5 Gal	0.7	0.3	0.2	19
H2 GlcNAc	1.0	0.4	0.4	32
H6 GlcNAc	0.8	0.3	0.3	24
H3 Gal	0.3	0.3	0.1	8
NHAc GlcNAc	1.0	0.4	0.4	31
H6 Gal	3.1	0.1	0.3	23

SUPPORTING FIGURES

Figure S1

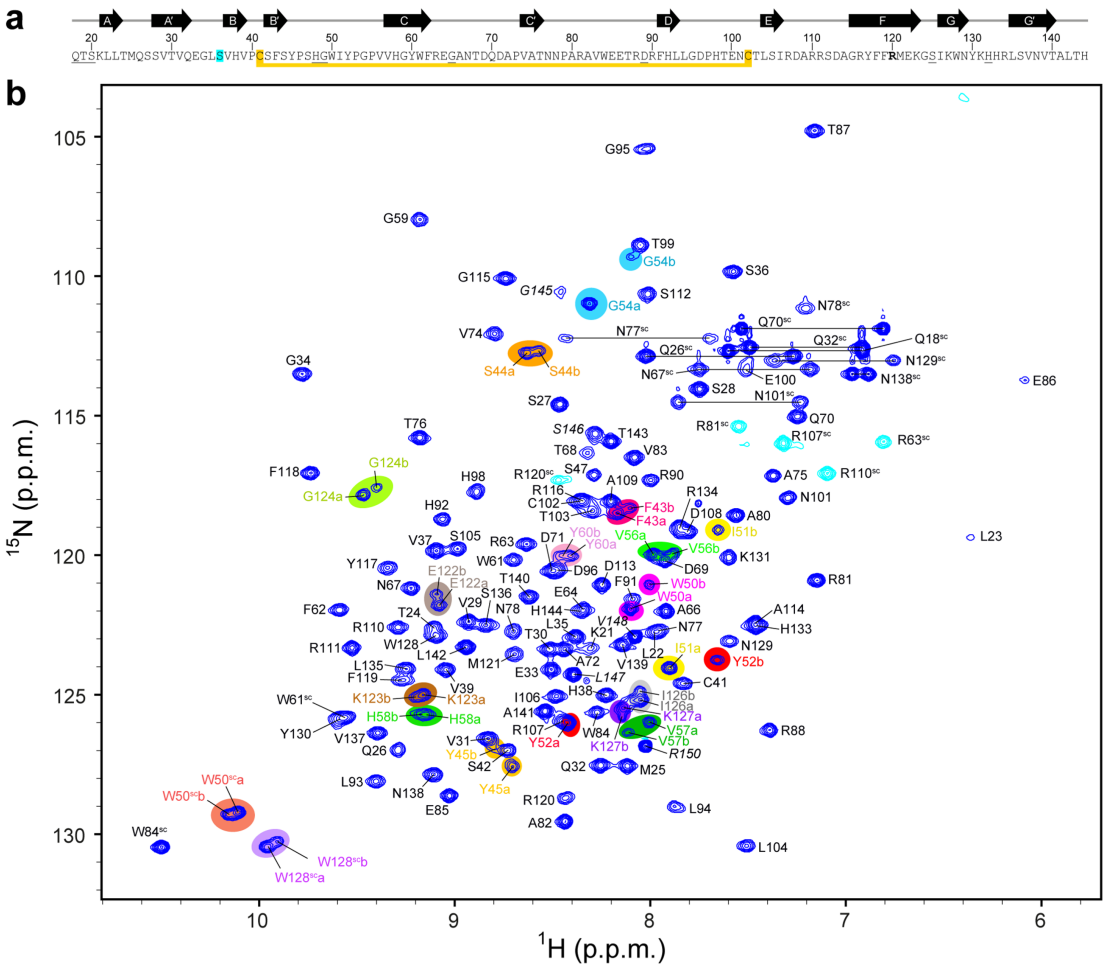

Figure S1. NMR backbone assignment of Siglec-9$_{d1}$. A) Amino acid sequence of Siglec-9$_{d1}$ (residues 18-144) construct used in this study. The predicted β-strands are depicted with black arrows on top of the amino acid sequence. The disulfide bond is indicated by a yellow line. B) ^{1}H-^{15}N HSQC spectrum of Siglec-9$_{d1}$ measured at 293 K with assignments. Signals with peak doubling are highlighed by different background colors, signals of the major set are labeled with an additional letter a, the minor set with a letter b.

Figure S2

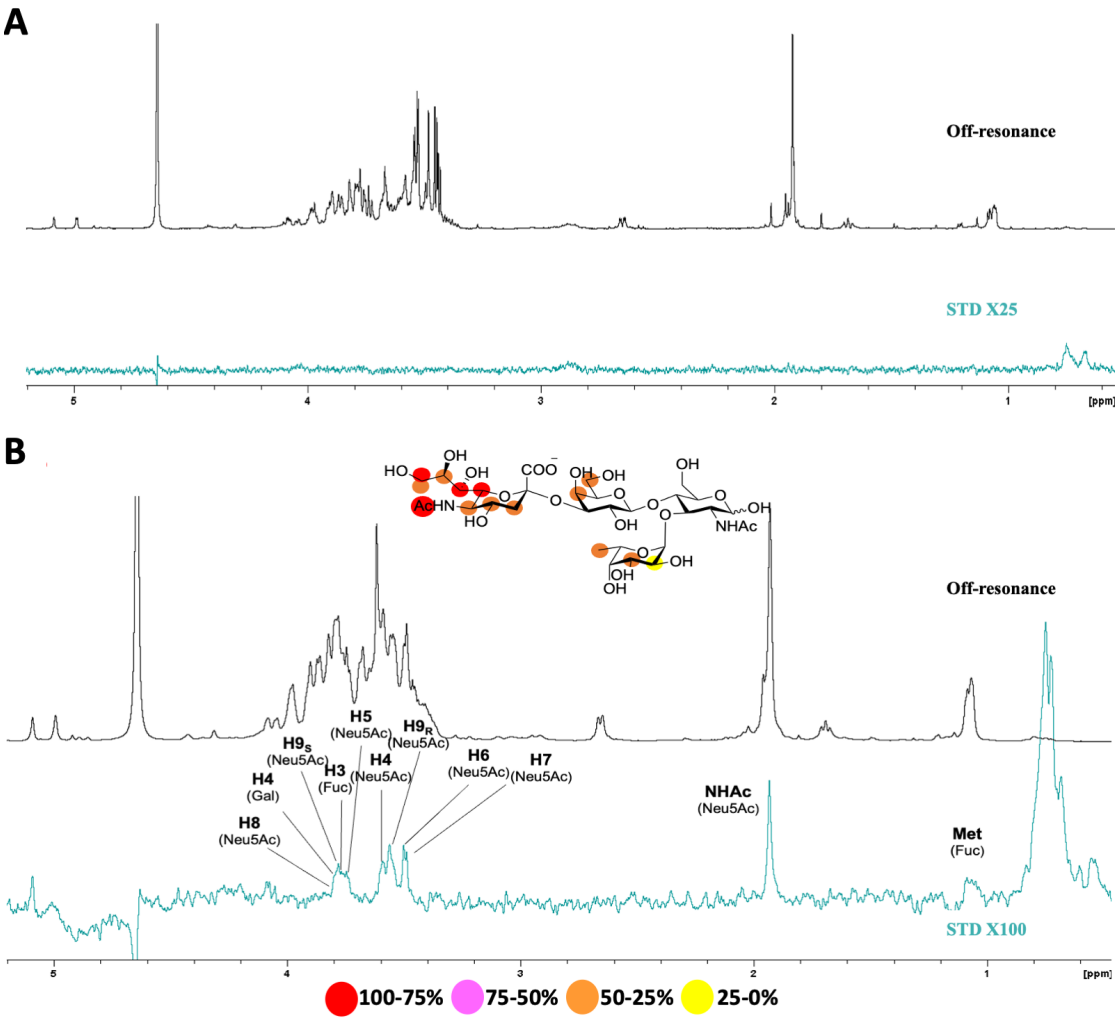

C

Protons	STD-AF	STD-AF (%)
NHAc Neu5Ac	0.36	100
H7 Neu5Ac	0.32	89
S9proR Neu5Ac	0.28	78
H6 Neu5Ac	0.27	76
H4 Neu5Ac	0.20	56
H9proS Neu5Ac	0.16	44
H5 Neu5Ac	0.16	44
H8 Neu5Ac	0.14	38
H3ax Neu5Ac	0.14	38
H6 Gal	0.12	33
Met Fuc	0.12	33
H3eq Neu5Ac	0.11	31
H4 Gal	0.11	31
H3 Fuc	0.10	27
H4 Fuc	0.06	16

Figure S2. STD-NMR epitope mapping of sLeX to mVENUS and Siglec-9$_{d1}$. A) Reference off-resonance spectrum (black) and STD-NMR spectra with 25 x amplification (cyan) of the mVENUS and sLeX in molar ratio of 1: 40 (mVENUS: ligand). B) Reference off-resonance spectrum (black) and STD-NMR spectra (100 x) (cyan) of the Siglec-9$_{d1}$ and sLeX in molar ratio of 1: 40 (Siglec-9: ligand). STD-based epitope mapping in sLeX is indicated. C) Epitope residues

of sLeX calculated from the ^{1}H STD-NMR experiment in the presence of Siglec-9_{d1} (1:40 molar ratio).

Figure S3

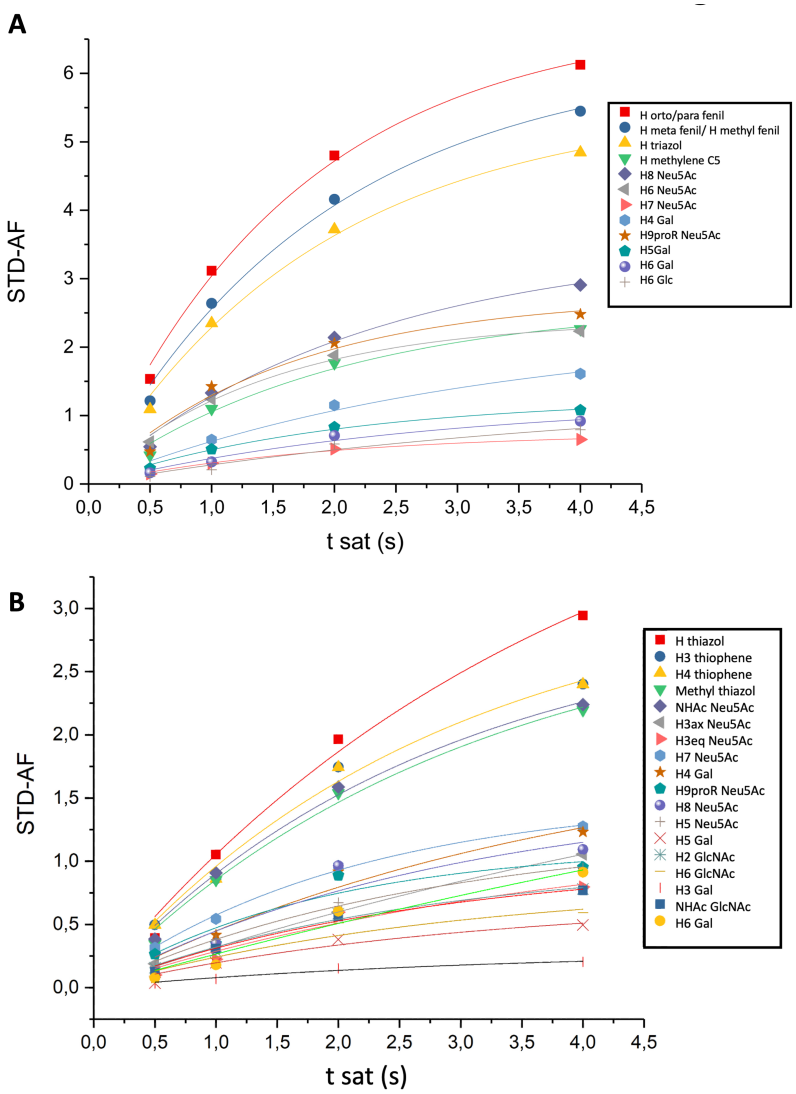

Figure S3. **^{1}H STD-NMR experiment for the complex formed by the modified sialogycans (^{BTC}Neu5Ac and ^{MTTS}Neu5Ac) and Siglec-9$_{d1d3}$.** A) ^{1}H STD-NMR experiment for the complex formed by ^{BTC}Neu5Ac and Siglec-9$_{d1d3}$ (1:40 molar ratio). B) ^{1}H STD-NMR experiment for the complex formed by ^{MTTS}Neu5Ac and Siglec-9$_{d1d3}$ (1:40 molar ratio). The intensities of STD signals obtained at different saturation times (0.5 s, 1 s, 2 s and 4 s) are plotted and fitted following the mono-exponential equation to obtain normalized STD signals, as explained in the materials and methods section.

Figure S4

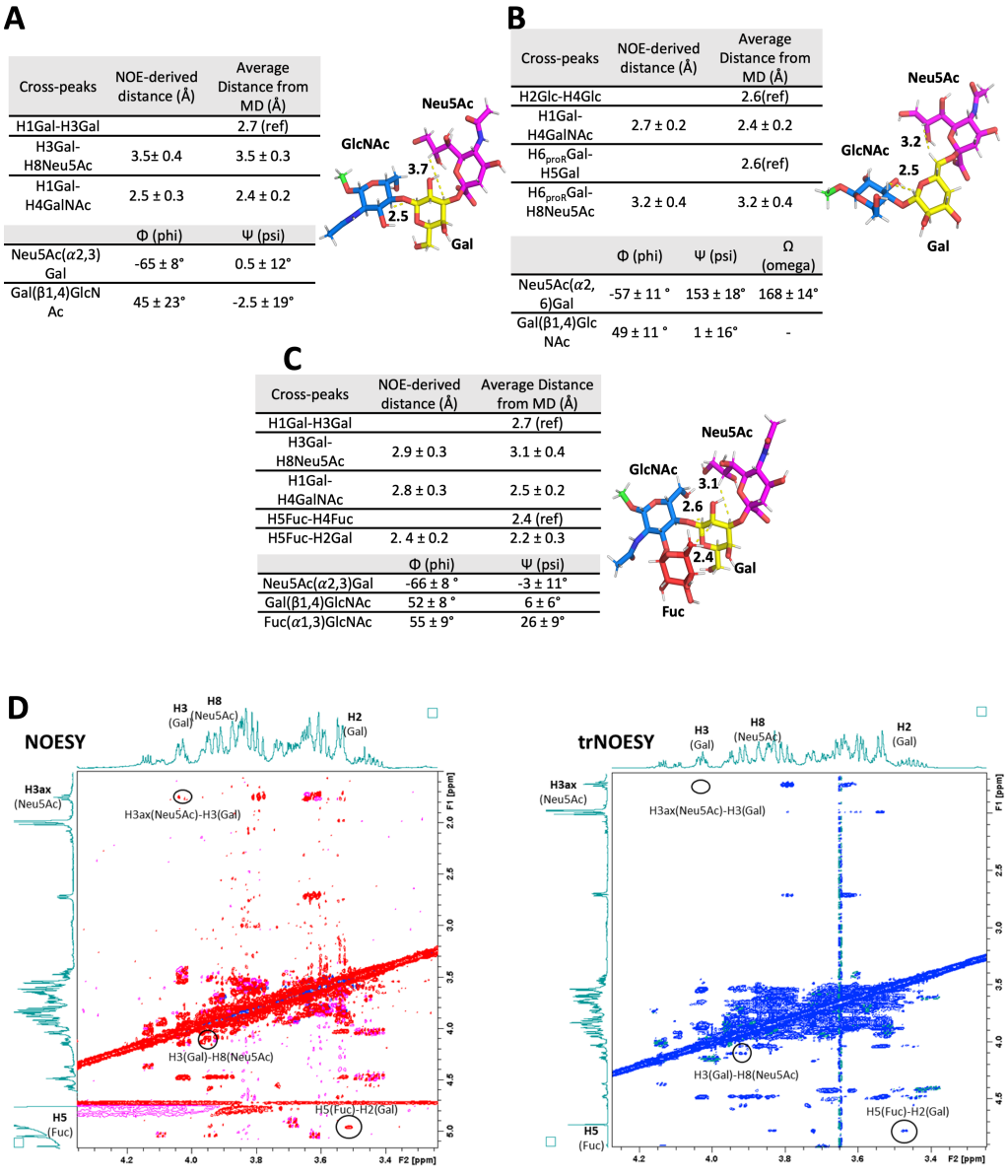

Figure S4. Conformation of α2,3SLN, α2,6SLN and sLeX in the presence of Siglec9$_{d1-d3}$. A) NOESY derived calculated distances for α2,3SLN in the presence of Siglec9$_{d1-d3}$ are shown in the Table. The binding pose of α2,3SLN is represented with sticks. B) NOESY derived calculated distances for α2,6SLN in the presence of Siglec9$_{d1-d3}$ and the binding pose of α2,6 SLN. C) NOESY derived calculated distances for sLeX. The dihedral angles of the *O*-glycosidic linkages were determined from the calculated distances (Table). D) NOESY spectra of sLeX is presented when free in solution (left, in red) and bound to Siglec-9$_{d1d3}$ (right, in blue). Key intermolecular cross-peaks are highlighted in brackets. Interproton distances were obtained by using the isolated spin pair approximation (ISPA) method.[10] NOE integrals were estimated to contain a 10% error. Thus, the ranges given for the NOE-derived distances were calculated based on this estimation.

Figure S5

A

Cross-peaks	NOE-derived distance (Å)	Average distance from MD (Å)
H3Gal-H4Gal		2.5 (ref)
H4Gal-$H3_{ax}$Neu5Ac	4.3 ± 0.4	4.1 ± 0.3
H5Gal-$H6_{proS}$Gal		2.4 (ref)
$H6_{proR}$Gal-$H3_{ax}$Neu5Ac	3.7 ± 0.3	4.1 ± 0.3
H5Gal- H1Gal		2.6 (ref)
H5Gal-$H3_{ax}$Neu5Ac	4.0 ± 0.4	4.2 ± 0.2
H4Glc-H1Gal	2.4 ± 0.2	2.5 ± 0.3
H5Gal-$H6_{proR}$Gal		2.6 (ref)
$H6_{proR}$Gal-H8Neu5Ac	2.8 ± 0.3	3.0 ± 0.3

	Φ (phi)	Ψ (psi)	Ω (omega)
Neu5Ac(α2,6) Gal	-62 ± 8 °	153 ± 9°	171 ± 9°
Gal(β1,4)Glc	45 ± 11 °	10 ± 11°	-

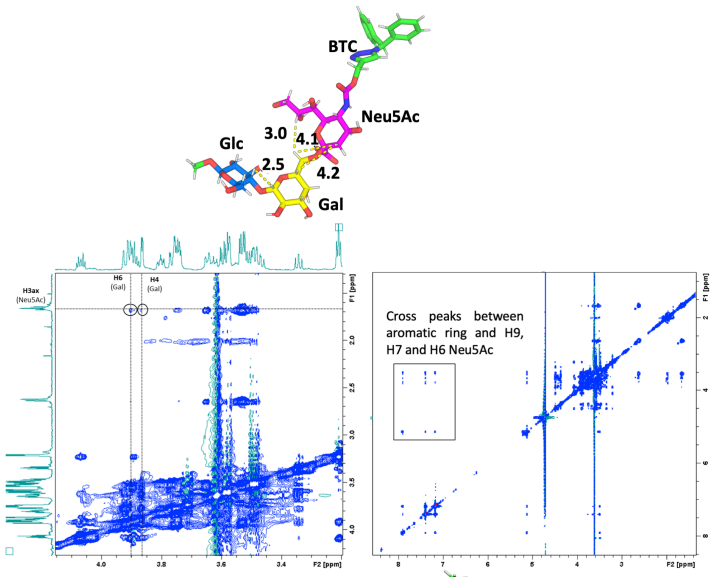

B

Cross-peaks	NOE-derived distance (Å)	Average distance from MD (Å)
H3-H4thiophene		2.6 (ref)
H4thiophene-H5thiazole	2.2 ± 0.2	2.2 ± 0.1
H8Neu5Ac-H3thiophene	3.6 ± 0.3	3.7 ± 0.3
$H9_{proS}$Neu5Ac-H3thiophene	3.1 ± 0.3	3.3 ± 0.2
$H9_{proR}$Neu5Ac-H3thiophene	3.0 ± 0.3	3.1 ± 0.2
H1Gal-H3Gal		2.6 (ref)
H1Gal-H4GlcNAc	2.7 ± 0.2	2.5 ± 0.2
H3Gal-H4Gal		2.5 (ref)
H4Gal-$H3_{ax}$Neu5Ac	4.3 ± 0.4	4.3 ± 0.3
H4Gal-$H3_{eq}$Neu5Ac	3.9 ± 0.3	3.6 ± 0.2
H5Gal-$H6_{proR}$Gal		2.6 (ref)
$H6_{proR}$Gal-H8Neu5Ac	3.0 ± 0.3	3.3 ± 0.4

	Φ (phi)	Ψ (psi)	Ω (omega)
Neu5Ac(α2,6) Gal	-53 ± 13 °	162 ±12°	171 ± 10°
Gal(β1,4)GlcNAc	45 ± 10 °	2 ± 12°	-

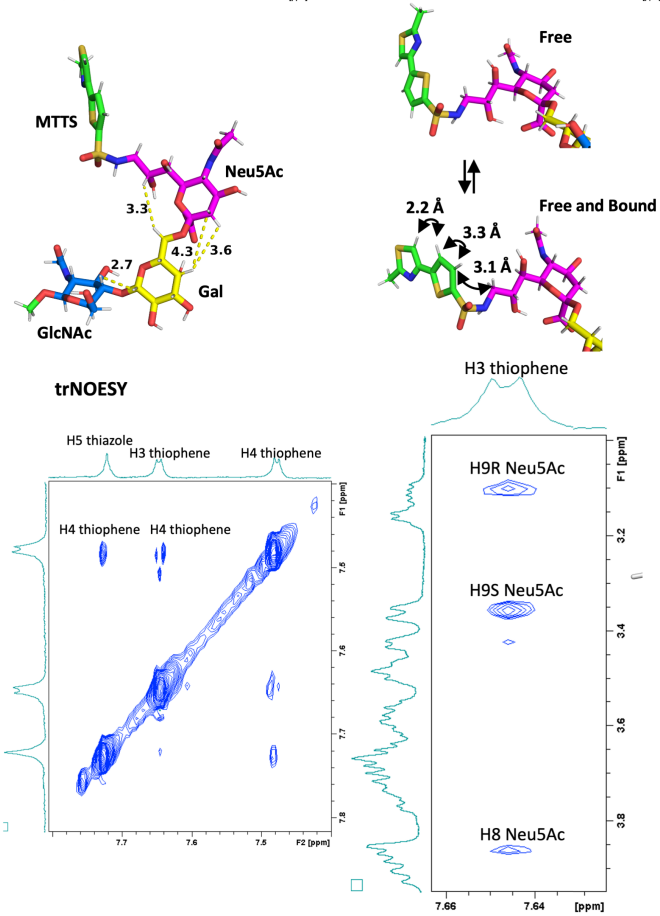

Figure S5. Conformation of ^{BTC}Neu5Ac and MTSSNeu5Ac bound to Siglec-9_{d1-d3}. A) From the calculated distances shown in the Table dihedral angles of the *O*-glycosidic linkages of ^{BTC}Neu5Ac were determined. Below, the NOESY spectra of ^{BTC}Neu5Ac in the presence of the Siglec9_{d1-d3} is shown. Cross-peaks between the aromatic ring and the H9, H7 and H6 of Neu5Ac are highlighted. These cross-peaks do not appear in the free NOESY spectrum but in the bound

form, as a consequence of the spin-diffusion effect due the intermolecular contacts between the W128 and the diphenylmethyl moiety of the glycomimetic. B) NOESY derived distances for ^{MTTS}Neu5Ac ligand. In the spectra below, NOESY spectra of the glycomimetic in the presence of the Siglec9$_{d1\text{-}d3}$ is shown. Key cross-peaks that only show up in the bound form and indicate the directionality of the heteroaromatic ring into binding site are highlighted. Interproton distances were obtained by using the isolated spin pair approximation (ISPA) method.[10] NOE integrals were estimated to contain a 10% error. Thus, the ranges given for the NOE-derived distances were calculated based on this estimation.

Figure S6

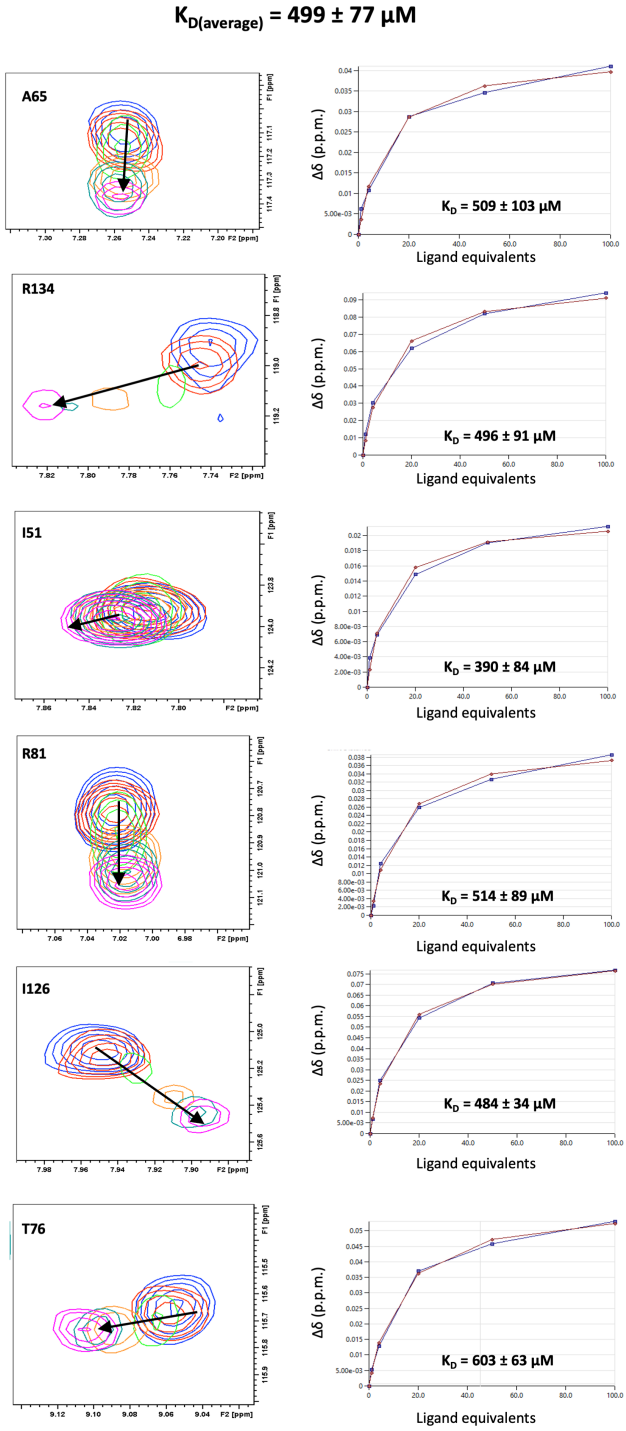

Figure S6. ^{1}H-^{15}N HSQC chemical shift perturbations induced by sLeX ligand. Highly perturbed residues are shown as well as their corresponding dissociation constants (K_D). The K_D of the ligands were calculated as described in Materials and Methods. CcpNmr Analysis software[11] was used to fit (in red) the curves of the obtained experimental data (in blue).

Figure S7

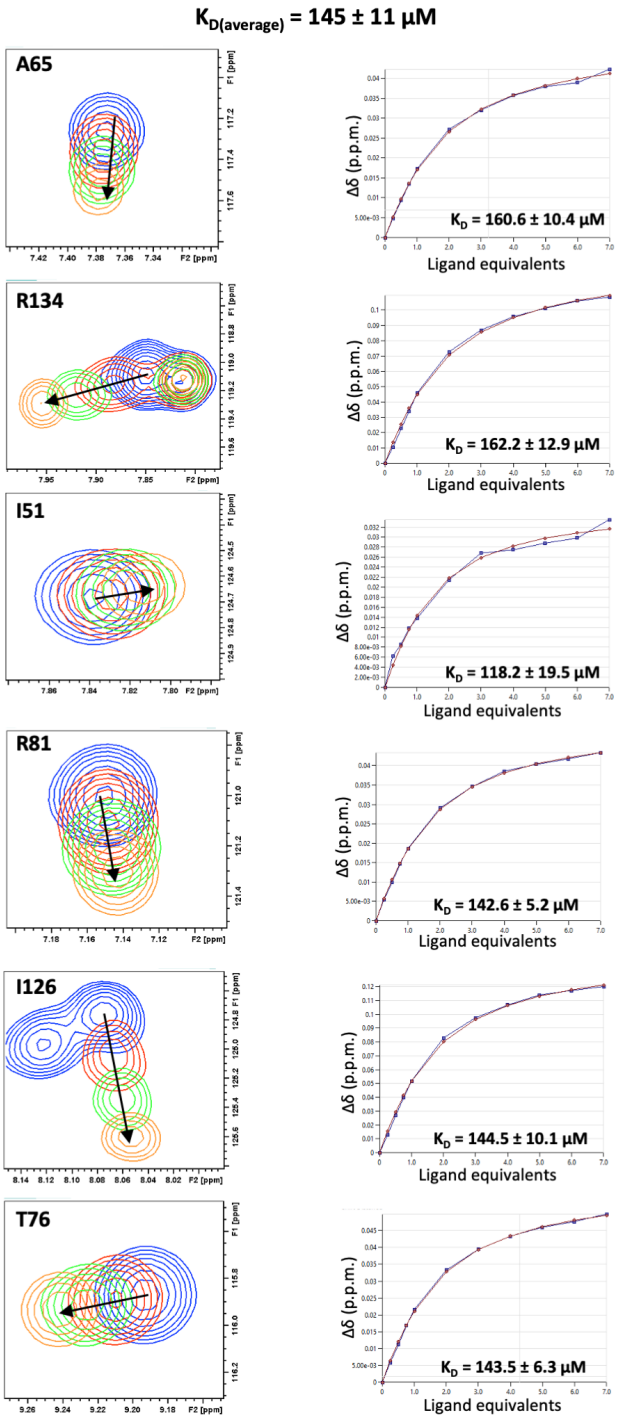

Figure S7. ^{1}H-^{15}N HSQC chemical shift perturbations induced by 6-*O*-sulfo sLeX ligand. Highly perturbed representative residues are shown as well as their corresponding dissociation constants. The K_D of the ligands were calculated as described in Materials and Methods. CcpNmr Analysis software[11] was used to fit (in red) the curves of the obtained experimental data (in blue).

Figure S8

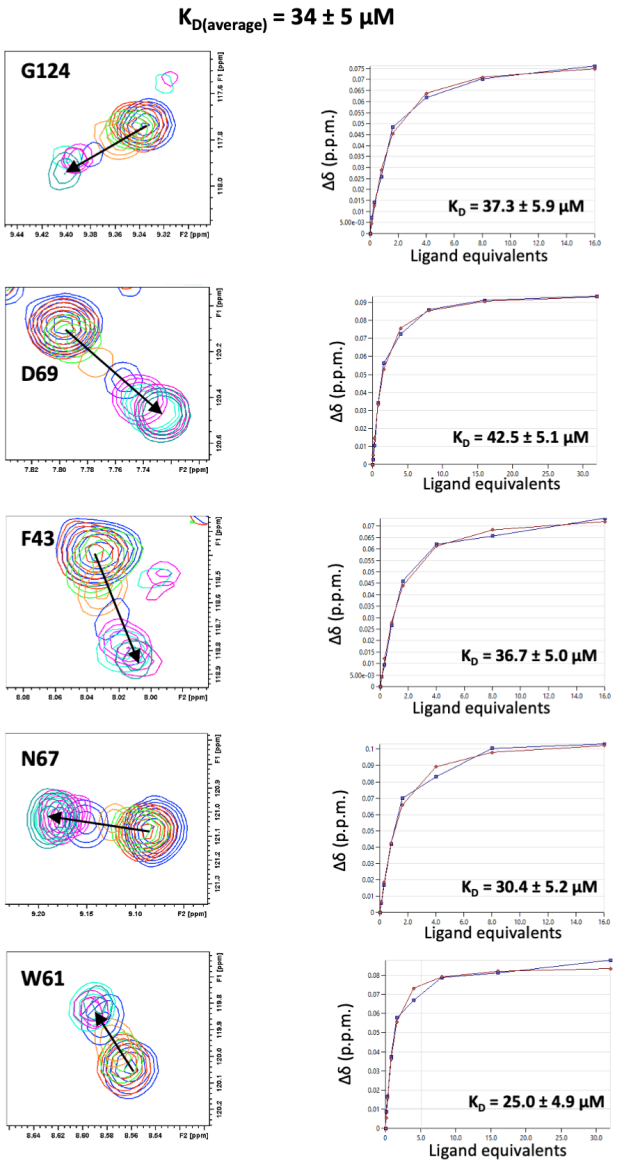

Figure S8. ^{1}H-^{15}N HSQC chemical shift perturbations induced by 6-*O*-sulfo ^{BTC}Neu5Ac. Highly perturbed representative residues are shown as well as their corresponding dissociation constants. CcpNmr Analysis software[11] was used to fit (in red) the curves of the obtained experimental data (in blue).

Figure S9

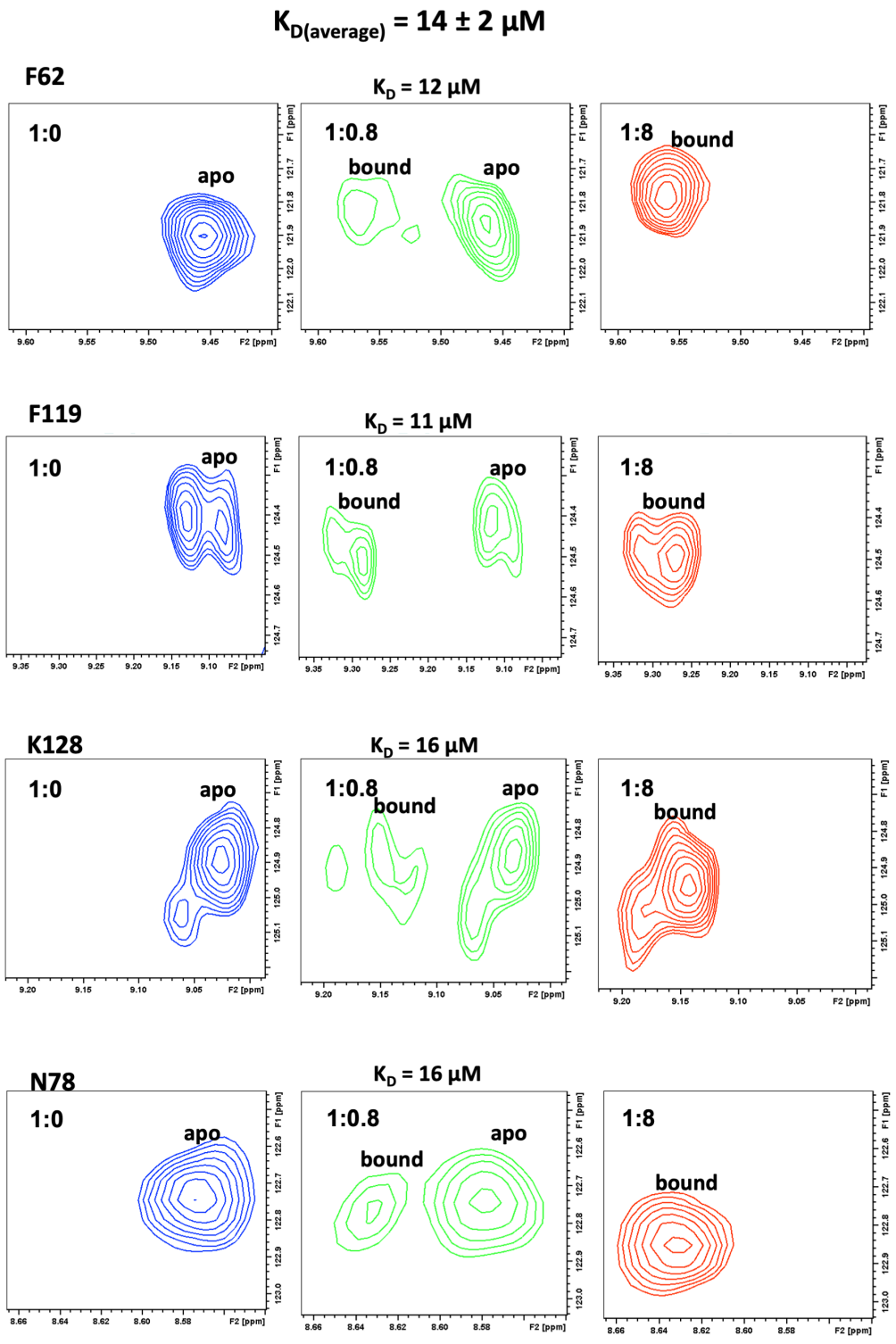

Figure S9. Determination of the dissociation constant (K_D) of ^{MTTS}Neu5Ac. In blue the ^{1}H-^{15}N HSQC cross-peaks of the indicated amino acids are shown. In green, at 0.8 equivalents of ligand, both apo and bound form can be observed simultaneously. In red, at 8 ligand equivalents, only the bound form can be observed). The K_D of the ligands were calculated as described in Materials and Methods.

Figure S10

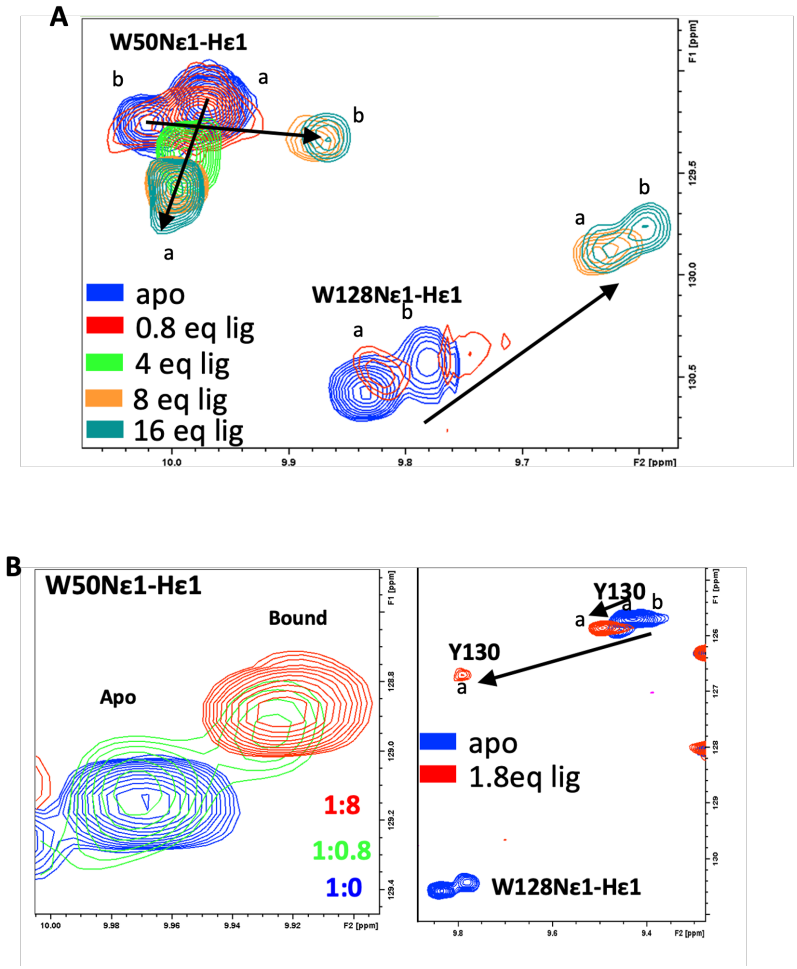

Figure S10. Specific ^{1}H-^{15}N HSQC chemical shift changes induced by the aromatic substitutions of ^{BTC}Neu5Ac and ^{MTTS}Neu5Ac ligands. A) Specific ^{1}H-^{15}N HSQC chemical shift changes induced by the aromatic substitutions of ^{BTC}Neu5Ac. Side chain NH groups of W50 and W128 are very affected by the presence of the 1-(diphenylmethyl)-1H-1,2,3-triazole moiety of the ligand. W128Nε1-Hε1 signals are heavily shifted and they do disappear at 4 ligand equivalents, for after being recovered at 8 equivalents. W50Nε1-Hε1 is also heavily perturbed. Even though the W50 backbone amide is perturbed almost twice as much as the standard deviation, the side chain amine of the indole shows higher perturbation. B) Specific ^{1}H-^{15}N HSQC chemical shift changes induced by the aromatic substitutions of ^{MTSS}Neu5Ac. Even though W50Nε1-Hε1 is in the slow-exchange regime, is 3-times less shifted than with the previous ^{BTC}Neu5Ac ligand. Unlike with the previous modified glycan, W128Nε1-Hε1 vanishes at 1.8 ligand equivalent addition. Additionally, Y130 is heavily shifted ($\Delta\delta^{1}_{H}$ = 0.36 ppm, $\Delta\delta^{15}_{N}$ = 0.91 ppm) caused by the substitutions of the ^{MTTS}Neu5Ac mimetic. The amino acids in the *cis* form are indicated with (a) while the ones in *trans* with (b).

Figure S11

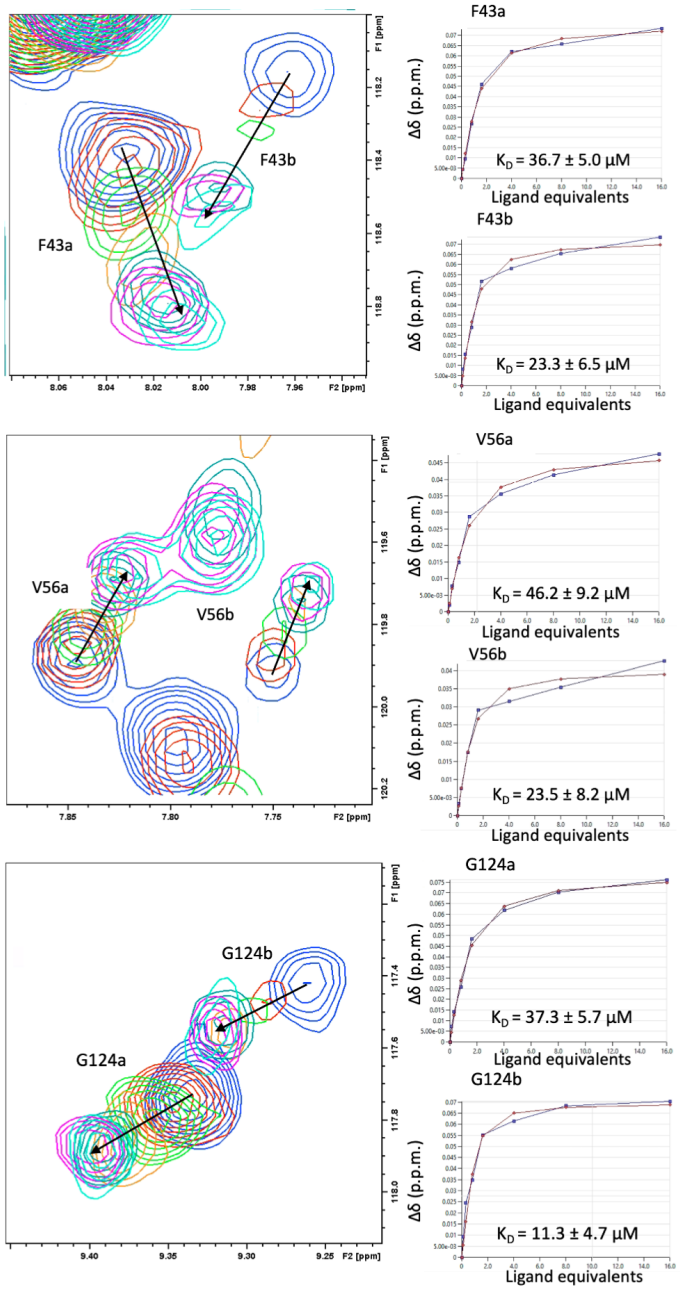

Figure S11. Chemical shift changes upon ^{BTC}Neu5Ac ligand addition of some of the doubled peaks in Siglec-9$_{d1}$ and their corresponding dissociation constant. Significant differences in the K_D were observed in the doubled peaks when the P53 from Siglec9$_{d1}$ is in the cis (a) and trans (b) form. CcpNmr Analysis software[11] was used to fit (in red) the curves of the obtained experimental data (in blue). The K_D of the ligands were calculated as described in Materials and Methods.

Figure S12

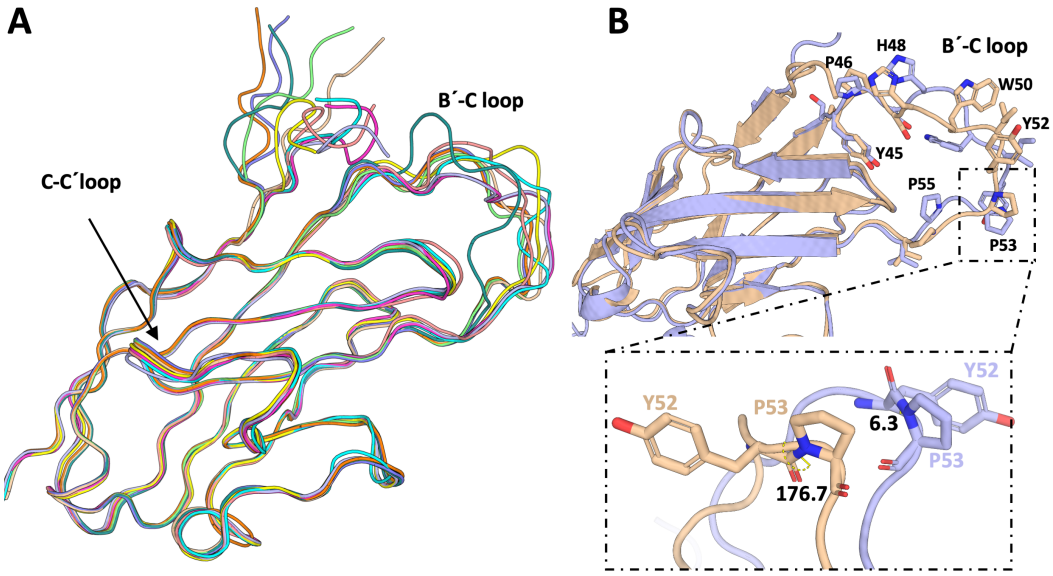

Figure S12. Comparison between the models of Siglec-9 V domain obtained by RoseTTA fold and AlphaFold. A) Superposition of the 5 best homology structures obtained with RoseTTA fold[12,13] and the 5 best obtained with AlphaFold [13,14]. All the given structures were identical except for the B´-C loop. B) Superposition of the best 3D structure models obtained with AlphaFold (in light blue) and RoseTTAFold (in wheat). The difference in the *cis* (modelled with AlphaFold) and *trans* (with RoseTTAFold) conformation of the P53 residue significantly affect the conformation adopted by the residues at the B´-C loop.

Figure S13

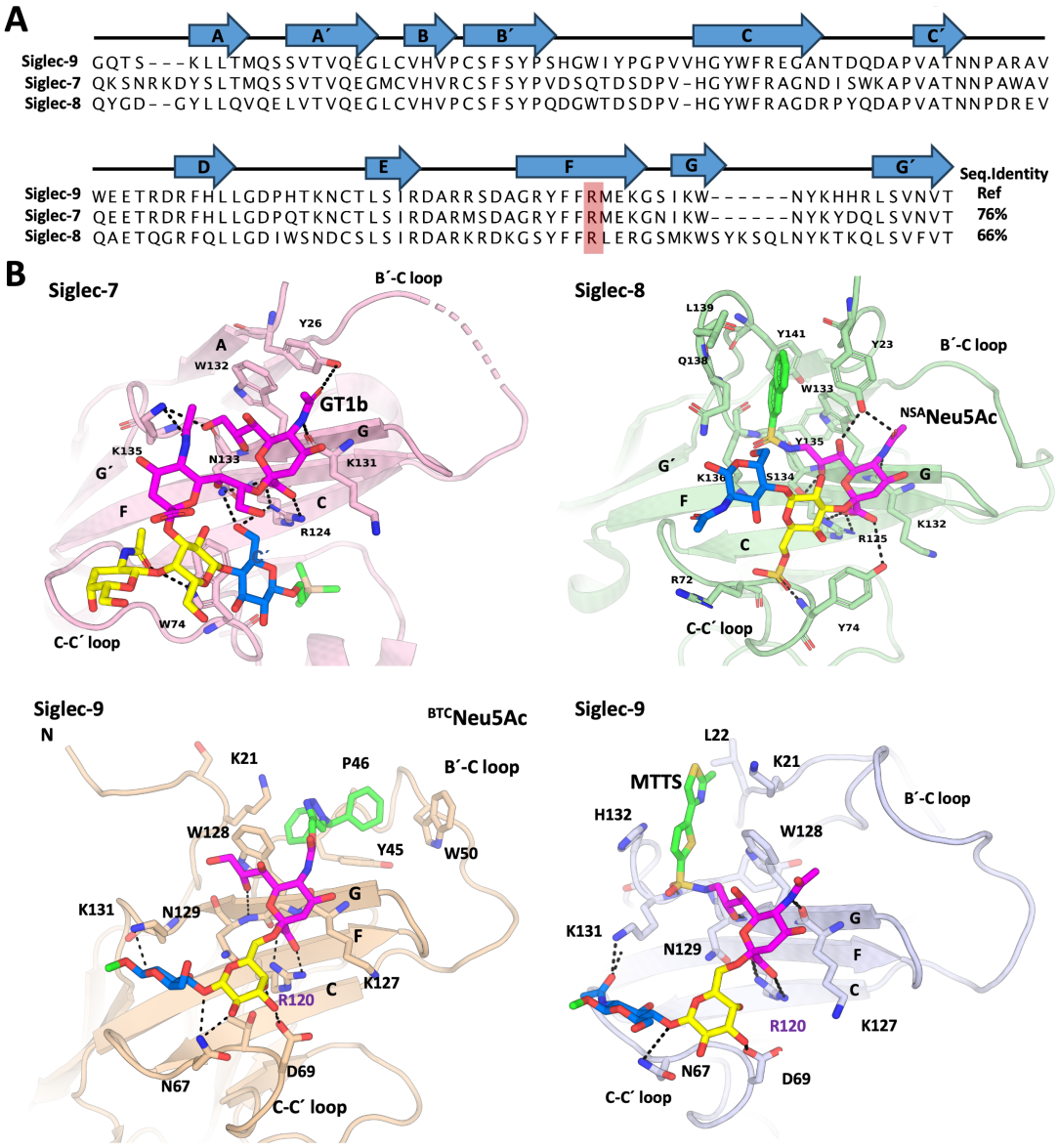

Figure S13. Comparison of the 3D structures of Siglec-7, Siglec-8 and the model of Siglec-9. A) Sequence alignment of the V-type domain of -7, -8 and -9. Siglec-9 secondary structure elements are represented at the top alignment. Conserved Arg involved in binding sialic acid is marked by a red box. Amino acid sequence identity between the V-type domains of Siglec-7 and -8 versus Siglec-9 reported as paired percent values. B) Cartoon representation of the crystal structure of Siglec-7 (in pink) in complex with GT1b (PDB ID: 2HRL), the crystal structure of Siglec-8 (in green) in complex with ^{NSA}Neu5Ac (PDB ID: 7QUI); and the model of Siglec-9 (*trans* model in wheat) in complex with ^{BTC}Neu5Ac and Siglec-9 (*cis* model in blue) ^{MTTS}Neu5Ac.

Figure S14

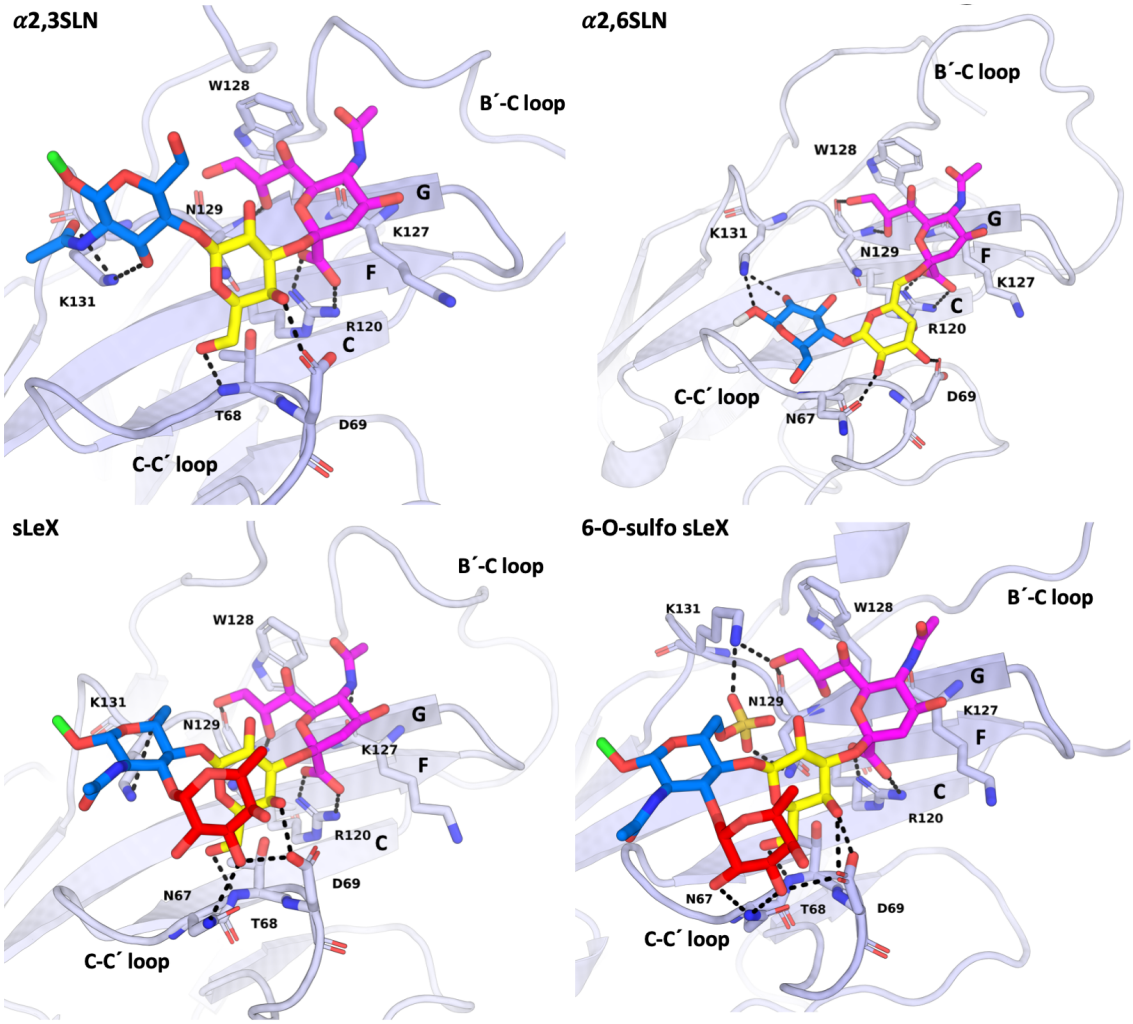

Figure S14. Representative binding modes of *α*2,3SLN, *α*2,6SLN, sLeX and 6-*O*-sulfo sLeX to Siglec-9.

Figure S15

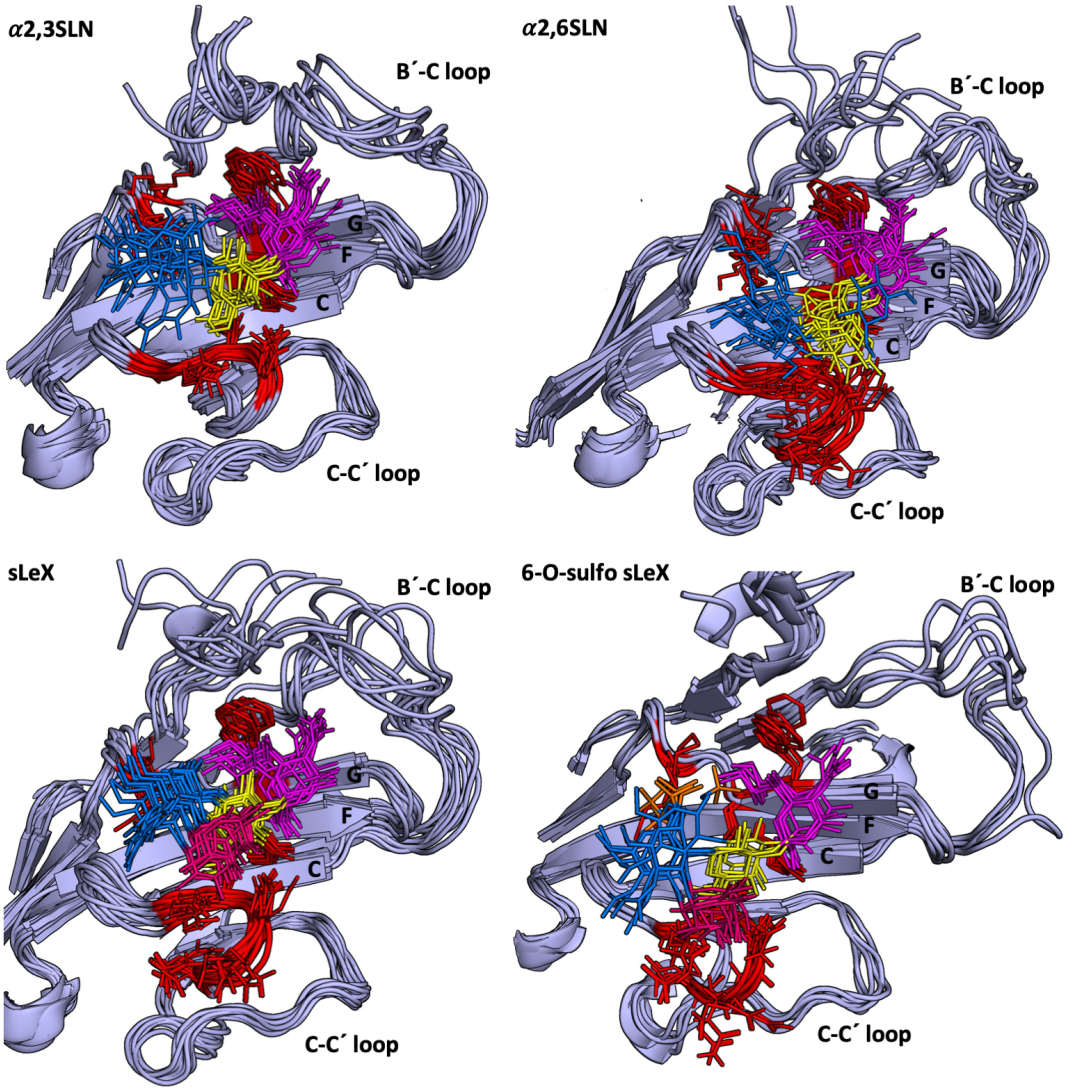

Figure S15. Superposition of the MD-based binding poses of natural glycans *α*2,3SLN, *α*2,6SLN, sLeX and 6-*O*-sulfo sLeX.

Figure S16

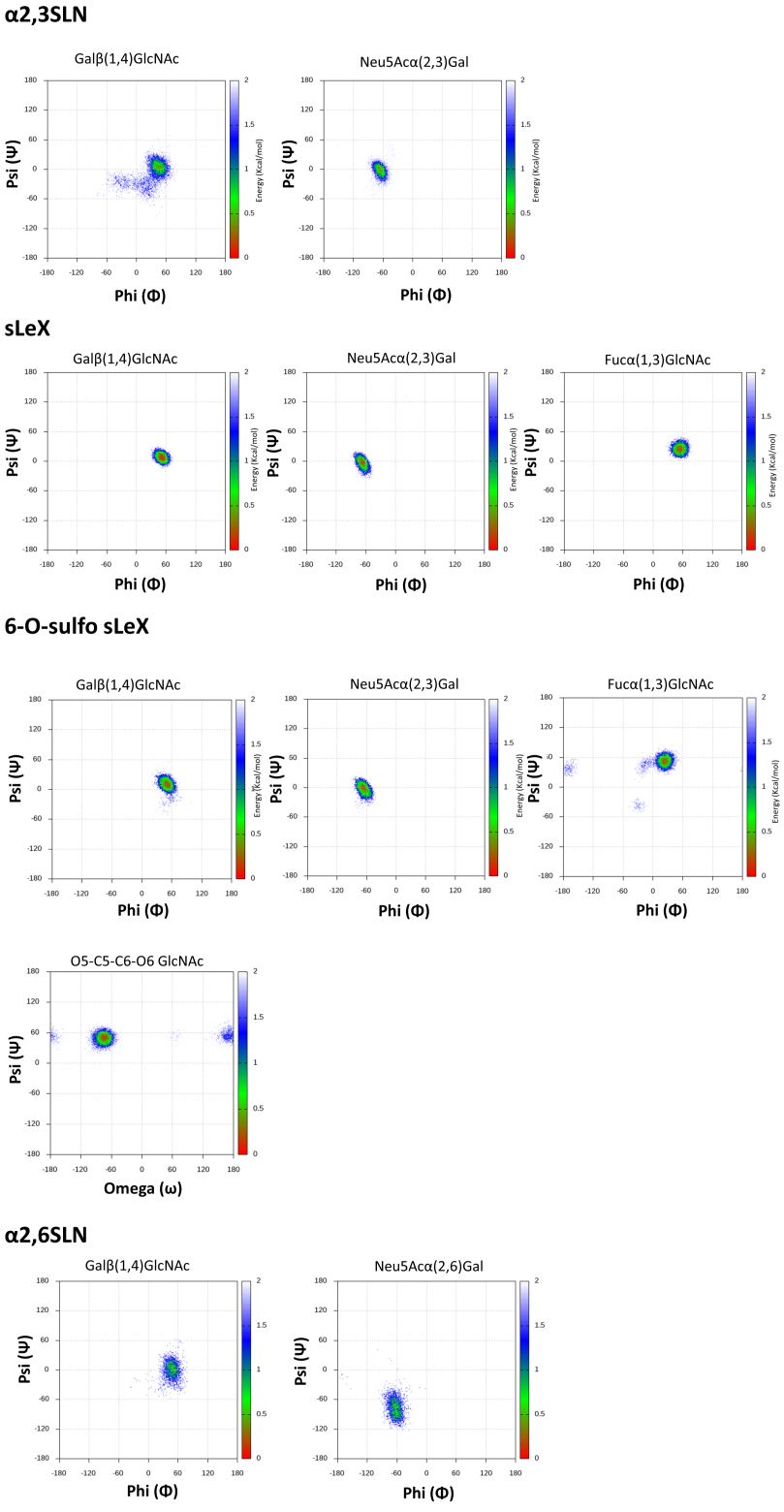

Figure S16. 2D histograms of the Φ (H_1'-C_1'-O_n -C_n) and Ψ (C_1'- O_n -C_n -H_n) dihedral angles of the *O*-glycosidic bond of the different natural glycans. Also, the ω (O_5-C_5-C_6-O_6) of the hydroxymethyl of 6-*O*-sulfo Glc*N*Ac dihedral is represented in the case of the 6-*O*-sulfo sLeX glycan.

Figure S17

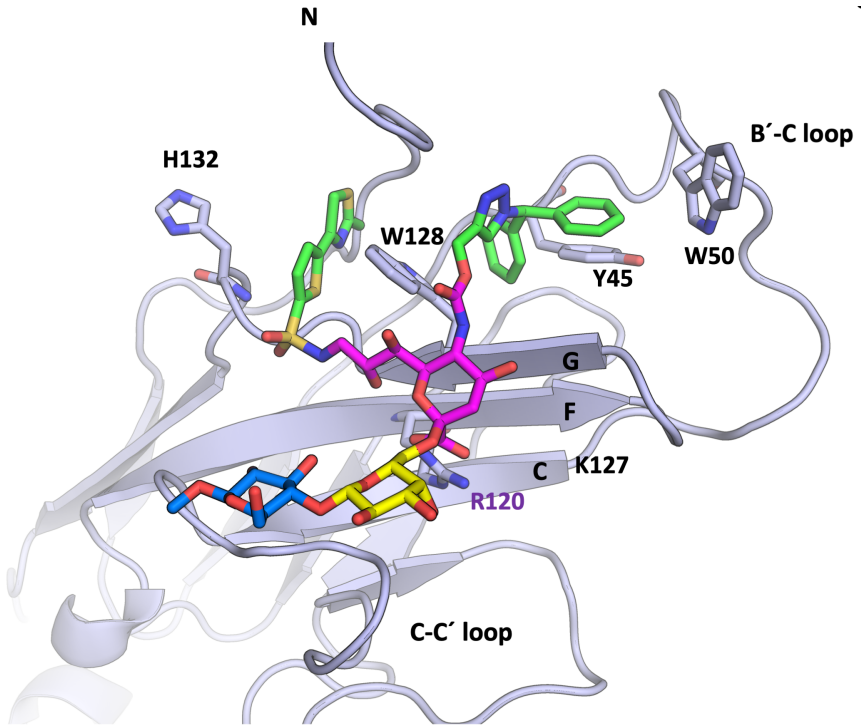

Figure S17. Three dimensional model of a glycan mimetic combining modifications of BTC and MTTS bound to Siglec-9.

Figure S18

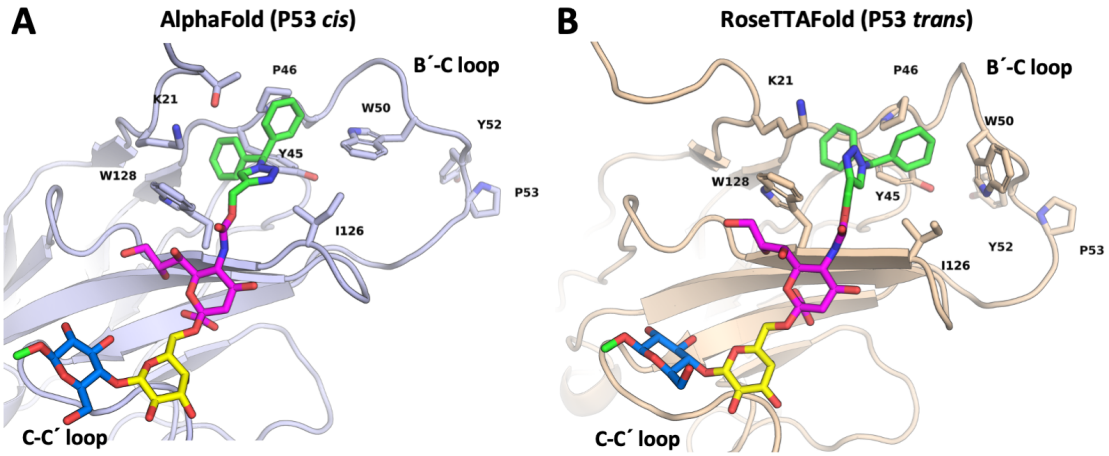

Figure S18. Representative binding poses of ^{BTC}Neu5Ac with the Siglec-9 structure from AlphaFold with Y52-P53 in *trans* (lightblue) and from RoseTTAFold with Y52-P53 in *trans* (wheat). A. Binding pose of ^{BTC}Neu5Ac within Siglec-9 at the *cis* form. **B**. Binding pose of ^{BTC}Neu5Ac within Siglec-9 at the *trans* form.

SUPPORTING REFERENCES

(1) Rillahan, C. D.; Schwartz, E.; McBride, R.; Fokin, V. V.; Paulson, J. C. Click and Pick: Identification of Sialoside Analogues for Siglec-Based Cell Targeting. *Angewandte Chemie* **2012**, *124* (44), 11176–11180. https://doi.org/10.1002/ANGE.201205831.

(2) Nycholat, C. M.; Duan, S.; Knuplez, E.; Worth, C.; Elich, M.; Yao, A.; O'Sullivan, J.; Mcbride, R.; Wei, Y.; Fernandes, S. M.; Zhu, Z.; Schnaar, R. L.; Bochner, B. S.; Paulson, J. C.; O'sullivan, J.; Mcbride, R.; Wei, Y.; Fernandes, S. M.; Zhu, Z.; Schnaar, R. L.; Bochner, B. S.; Paulson, J. C. A Sulfonamide Sialoside Analogue for Targeting Siglec-8 and-F on Immune Cells. *J Am Chem Soc* **2019**, *141* (36), 14032–14037. https://doi.org/10.1021/jacs.9b05769.

(3) Pröpster, J. M.; Yang, F.; Rabbani, S.; Ernst, B.; Allain, F. H.-T.; Schubert, M. Structural Basis for Sulfation-Dependent Self-Glycan Recognition by the Human Immune-Inhibitory Receptor Siglec-8. *Proceedings of the National Academy of Sciences* **2016**, *113* (29). https://doi.org/10.1073/pnas.1602214113.

(4) Pröpster, J. M.; Yang, F.; Ernst, B.; Allain, F. H. T.; Schubert, M. Functional Siglec Lectin Domains from Soluble Expression in the Cytoplasm of Escherichia Coli. *Protein Expr Purif* **2015**, *109*, 14–22. https://doi.org/10.1016/J.PEP.2015.01.005.

(5) Pröpster, J. M.; Yang, F.; Ernst, B.; Allain, F. H. T.; Schubert, M. Functional Siglec Lectin Domains from Soluble Expression in the Cytoplasm of Escherichia Coli. *Protein Expr Purif* **2015**, *109*, 14–22. https://doi.org/10.1016/j.pep.2015.01.005.

(6) Nagai, T.; Ibata, K.; Park, E. S.; Kubota, M.; Mikoshiba, K.; Miyawaki, A. A Variant of Yellow Fluorescent Protein with Fast and Efficient Maturation for Cell-Biological Applications. *Nat Biotechnol* **2002**, *20* (1). https://doi.org/10.1038/nbt0102-87.

(7) Aricescu, A. R.; Lu, W.; Jones, E. Y. A Time- and Cost-Efficient System for High-Level Protein Production in Mammalian Cells. *Acta Crystallogr D Biol Crystallogr* **2006**, *62* (10), 1243–1250. https://doi.org/10.1107/S0907444906029799.

(8) Mayer, M.; Meyer, B.; Park, K. C.; Meunier, S. J.; Zanini, D.; Roy, R.; Lett, C.; Romanowska, A.; Meyer, B.; Mayer, D.-C. M. Characterization of Ligand Binding by Saturation Transfer Difference NMR Spectroscopy. *Wiley Online Library* **1999**, *38* (12), 5907–5908.

(9) Meyer, B.; Peters, T. NMR Spectroscopy Techniques for Screening and Identifying Ligand Binding to Protein Receptors. *Angewandte Chemie International Edition* **2003**, *42* (8), 864–890. https://doi.org/10.1002/ANIE.200390233.

(10) Gronenborn, A. M.; Clore, G. M. Investigation of the Solution Structures of Short Nucleic Acid Fragments by Means of Nuclear Overhauser Enhancement Measurements. *Prog Nucl Magn Reson Spectrosc* **1985**, *17*, 1–32. https://doi.org/10.1016/0079-6565(85)80004-2.

(11) Vranken, W. F.; Boucher, W.; Stevens, T. J.; Fogh, R. H.; Pajon, A.; Llinas, M.; Ulrich, E. L.; Markley, J. L.; Ionides, J.; Laue, E. D. The CCPN Data Model for NMR Spectroscopy: Development of a Software Pipeline. *Proteins: Structure, Function and Genetics* **2005**, *59* (4), 687–696. https://doi.org/10.1002/prot.20449.

(12) Baek, M.; DiMaio, F.; Anishchenko, I.; Dauparas, J.; Ovchinnikov, S.; Lee, G. R.; Wang, J.; Cong, Q.; Kinch, L. N.; Dustin Schaeffer, R.; Millán, C.; Park, H.; Adams, C.; Glassman, C. R.; DeGiovanni, A.; Pereira, J. H.; Rodrigues, A. V.; Van Dijk, A. A.; Ebrecht, A. C.; Opperman, D. J.; Sagmeister, T.; Buhlheller, C.; Pavkov-Keller, T.; Rathinaswamy, M. K.; Dalwadi, U.; Yip, C. K.; Burke, J. E.; Christopher Garcia, K.; Grishin, N. V.; Adams, P. D.; Read, R. J.; Baker, D. Accurate Prediction of Protein Structures and Interactions Using a Three-Track Neural Network. *Science (1979)* **2021**, *373* (6557), 871–876. https://doi.org/10.1126/SCIENCE.ABJ8754/SUPPL_FILE/ABJ8754_MDAR_REPRODUCIBILITY_CHECKLIST.PDF.

(13) Mirdita, M.; Schütze, K.; Moriwaki, Y.; Heo, L.; Ovchinnikov, S.; Steinegger, M. ColabFold: Making Protein Folding Accessible to All. *Nature Methods 2022 19:6* **2022**, *19* (6), 679–682. https://doi.org/10.1038/s41592-022-01488-1.

(14) Jumper, J.; Evans, R.; Pritzel, A.; Green, T.; Figurnov, M.; Ronneberger, O.; Tunyasuvunakool, K.; Bates, R.; Žídek, A.; Potapenko, A.; Bridgland, A.; Meyer, C.; Kohl, S. A. A.; Ballard, A. J.; Cowie, A.; Romera-Paredes, B.; Nikolov, S.; Jain, R.; Adler, J.; Back, T.; Petersen, S.; Reiman, D.; Clancy, E.; Zielinski, M.; Steinegger, M.; Pacholska, M.; Berghammer, T.; Bodenstein, S.; Silver, D.; Vinyals, O.; Senior, A. W.; Kavukcuoglu, K.; Kohli, P.; Hassabis, D. Highly Accurate Protein Structure Prediction with AlphaFold. *Nature* **2021**, *596* (7873). https://doi.org/10.1038/s41586-021-03819-2.